Cooperative Path Following of Multiple Multirotors over Time-Varying Networks

Venanzio Cichella, Isaac Kaminer, Vladimir Dobrokhodov, Enric Xargay, Ronald Choe, Naira Hovakimyan, A. Pedro Aguiar, and António M. Pascoal

***Abstract*—This paper addresses the problem of time-coordination of a team of cooperating multirotor unmanned aerial vehicles that exchange information over a supporting time-varying network. A distributed control law is developed to ensure that the vehicles meet the desired temporal assignments of the mission, while flying along predefined collision-free paths, even in the presence of faulty communication networks, temporary link losses, and switching topologies. In this paper the coordination task is solved by reaching consensus on a suitably defined coordination state. Conditions are derived under which the coordination errors converge to a neighborhood of zero. Simulation and flight test results are presented to validate the theoretical findings.**

***Note to Practitioners*—This paper presents an approach which enables a fleet of multirotor UAVs to follow a set of desired trajectories and coordinate along them, thus satisfying specific spatial and temporal assignments. The proposed solution can be employed in applications in which multiple vehicles are tasked to execute cooperative, collision-free maneuvers, and accomplish a common goal in a safely manner. An example is sequential monitoring, in which the UAVs have to visit and monitor a set of points of interest, while maintaining a desired temporal separation between each other. In this paper we also simulate a scenario in which the vehicles, positioned in a square room, are required to exchange position with each other. It is shown that the proposed control algorithm not only ensures that the UAVs arrive at the final destinations at the same time, but also guarantees safety, i.e. the vehicles avoid collision with each other at all times.**

***Index Terms*—Time-coordinated path following, consensus algorithms, networked systems.**

I. Introduction

COOPERATION among multiple unmanned vehicles is an extremely challenging topic from a theoretical and practical standpoint, with far reaching implications in scientific and commercial mission scenarios. For this reason, in recent years the topic has been the subject of considerable research and development effort, especially in terms of control and communication technologies. Relevant work includes spacecraft formation flying [1]–[3], UAV control [4], [5], coordinated control of land robots [6]–[8], and control of multiple autonomous underwater vehicles [9], [10]. Research on cooperative flight of multirotor teams is particularly extensive (see [2], [3], [11]–[16] and references therein). In this context, the literature is mainly divided into two categories: *centralized* and *decentralized* cooperative control. In the first case, each vehicle is driven along its own predefined time-dependent trajectory, provided by a central unit (controller). In the latter, each UAV runs its own guidance, navigation, and control algorithms, and is thus able to autonomously react to the behavior of other vehicles and/or unforeseen events to safely reach a mutual goal [15]–[20]. In the context of small multirotor UAVs (often featuring CPUs with relatively small capabilities) a *hybrid* (mix of centralized and decentralized) control can be applied to significantly reduce the exchange of information between the central controller and the UAVs.

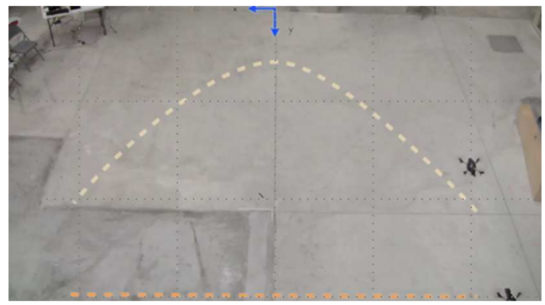

Fig. 1. Two quadrotors following two trajectories of different lengths while coordinating along the x-axis. A video of the flight test is available at https://www.youtube.com/watch?v=izXmgetsBYw.

However, performance of decentralized and hybrid cooperative controllers depends on the ability of the fleet to exchange information in a timely and reliable manner. Therefore, the quality of service of the supporting communication network plays a crucial role. As pointed out in [21], [22], in many scenarios the flow of information among vehicles may be severely restricted, either for security reasons or because of tight bandwidth limitations. As a consequence, no vehicle may be able to communicate with the entire fleet, and the amount of information that can be exchanged may be limited.

Motivated by previous results obtained by the same authors [23], this paper addresses the problem of coordinating a fleet of multirotor UAVs in the presence of communication constraints. In particular, the cooperative missions considered require that each vehicle follow a feasible collision-free path, and that all vehicles arrive at their respective final destinations at the

Venanzio Cichella, Enric Xargay, Ronald Choe and Naira Hovakimyan are with the Coordinated Science Laboratory, University of Illinois at Urbana-Champaign, Urbana, IL, 61801, USA. e-mail: {cichell2, xargay, choe19, nhovakim}@illinois.edu.

Isaac Kaminer and Vladimir Dobrokhodov are with the Department of Mechanical and Aerospace Engineering, Naval Postgraduate School, Monterey, CA, 93943, USA e-mail: {kaminer, vldobr}@nps.edu

A. Pedro Aguiar is with the Dept. of Electrical and Computer Engineering, Faculty of Engineering, University of Porto (FEUP), Porto, Portugal. e-mail: pedro.aguiar@fe.up.pt

António M. Pascoal is with the Institute for Systems and Robotics (ISR), Instituto Superior Tecnico (IST), Univ. Lisbon, Portugal. e-mail: antoniog@isr.ist.utl.pt

same time, or at different times so as to meet a desired inter-vehicle schedule. A simple example of coordination between two quadrotors is shown in Figure 1, where the vehicles are required to follow two paths of different lengths while coordinating along the x-axis. In this paper we aim at providing a solution which —differently from other works in the literature [2], [3], [8], [15], [16]— tackles the problem of decentralized cooperative control with time-varying communication networks through a Lyapunov-based approach, thus providing rigorous performance bounds as a function of the quality of service of the communication network. Moreover, we address the problem of non-ideal tracking performance of the UAVs, by showing that the time-coordination guarantees are retained even when the UAV does not converge –but remains close– to the desired position.

The present paper departs from previous results obtained by the research group in cooperative path-following control in a fundamental way. In [23] the authors presented path-following[1] and time-coordination algorithms that enable a fleet of fixed-wing UAVs to follow predefined spatial paths and synchronize along them. One of the main benefits of this framework lies in the fact that the speed of the vehicles can be adjusted online to synchronize the vehicles, as opposed to the coordinated trajectory-tracking approach where the coordination task is solved offline, and thus the control algorithm cannot adapt to external disturbances or vehicles' tracking errors. In [23], the path-following controller is designed so as to align the velocity vector of the UAV with the local tangent vector of the desired path, and it relies on the assumption that the speed of the vehicle is lower bounded by a positive constant [23, Equation (9)]. On the other hand, time-coordination is achieved by varying the speed of the vehicles involved in the mission. One of the key steps in the approach proposed in [23] lies in the design of the path-following solution (see [23, Section IV]), which significantly reduces the complexity of the problem at hand by reducing the coordination dynamics to n simple integrators, where n is the number of UAVs. However, while [23] offers an appealing solution for the cooperative control of fixed-wing UAVs, it cannot be employed when dealing with unmanned vehicles that allow the existence of zero velocity vectors (e.g. UAVs who can hover, such as multirotors). This limitation motivated us to reformulate the coordination problem in a different way. The goal of this paper is to provide a new solution to the time-coordination problem which is more general, and can be applied to a broader set of vehicles with different dynamics. In the approach proposed here, the *path-following* and the *time-coordination* problems are decoupled. At the path-following level, we assume that a control law capable of steering a multirotor along its assigned path is given. At the time-coordination level, the synchronization problem is solved by adjusting a new set of suitably defined coordination variables,

[1]Path-following: the underlying assumption in the path-following approach is that the path-following controller enables the vehicle to follow a geometric path, independently of the temporal assignments of the mission. This approach is thus in contrast to trajectory-tracking control, where the objective is to follow a predefined trajectory with a given timing law [24]. Therefore, in path-following control one can exploit the progression of the desired reference along the given path to achieve other objectives.

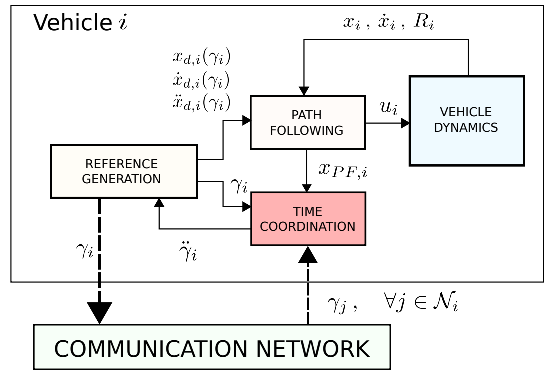

Fig. 2. Cooperative Path-Following of Multiple Multirotors over Time-Varying Networks. General Framework. Control Blocks and Interaction Between Them.

thus achieving vehicles' coordination. It is shown that the solution to the time-coordination problem exhibits guaranteed performance in the presence of time-varying communication networks, that arise due to temporary loss of communication links and switching communication topologies.

This paper is organized as follows: in Section II we introduce the general framework adopted; in Section III we describe the time-coordination problem by giving a suitable set of coordination variables and a set of assumptions that the communication network must satisfy; in Section IV we formulate the main results of this paper; simulation results are discussed in Section V, while flight test results are shown in Section VI; finally, in Section VII the main conclusions are presented.

II. General Framework

In this section, a general framework for cooperative path-following control of multirotors is introduced. The general framework builds on the approach to multi-vehicle cooperative control presented in previous work [25].

Given a multi-vehicle cooperative mission, a *trajectory-generation* algorithm produces a set of feasible spatial paths in 3D space together with a set of feasible speed profiles. A *path-following* controller allows each vehicle to converge to and follow its assigned path with the desired speed profile. A *time-coordination* control algorithm adjusts (indirectly) the progression of each vehicle along the path in order to achieve inter-vehicle coordination. Figure 2 presents the architecture. As mentioned earlier, this paper focuses on the problem of time-coordination. However, for the clarity of presentation, in this section we briefly describe the *trajectory-generation* and the *path-following* problems. For further details, the reader is referred to [26]–[28], where the authors tackle the trajectory-generation and path-following problems.

A. Trajectory Generation

At the trajectory-generation level, the objective is to plan a set of desired collision-free trajectories, which must be tracked by the vehicles. The algorithm can be summarized in two main steps:

a) first, a *trajectory-generation* algorithm produces a set of feasible geometric paths together with desired speed profiles. The problem at hand is to generate a set of n 3D time-trajectories that together minimize a given cost function (e.g. overall energy spent or time to maneuver), do not violate dynamic constraints of the vehicles, ensure that the vehicles maintain a predefined spatial clearance, and satisfy pre-specified mission-specific constraints. Given a cooperative mission of interest involving n vehicles, the problem of trajectory-generation can be formally stated as follows:

Problem 1 (Trajectory-Generation Problem): Find a set of n 3D time-trajectories $x_{d,i} : [0, t^*_{d,i}] \to \mathbb{R}^3$, $i \in \{1, \dots, n\}$, conveniently parameterized by a single time-variable $t_d \in [0, t^*_{d,i}]$, $t^*_{d,i} > 0$, satisfying:

- dynamic constraints:
$$0 \le v_{i,\min} < v_{d_i,\min} \le ||x'_{d,i}(t_d)|| \le v_{d_i,\max} < v_{i,\max} \,, \tag{1a}$$
$$||x''_{d,i}(t_d)|| \le a_{d_i,\max} < a_{i,\max} \,, \tag{1b}$$
where $x'_{d,i}(t_d)$ and $x''_{d,i}(t_d)$ are the desired linear speed and acceleration at t_d, and $v_{i,\min}$, $v_{i,\max}$ and $a_{i,\max}$ are the dynamic constraints of the i-th vehicle (minimum and maximum speed and maximum absolute value of the acceleration, respectively);
- simultaneous arrival at predefined destinations:
$$t^*_{d,i} = t^*_{d,j} = t^*_d \qquad \text{for} \quad i,j = 1,2,\dots,n \,; \tag{2}$$
- temporal separation between the paths:
$$\min_{\substack{i,j=1,\dots,n \\ i \ne j}} \|x_{d,i}(t_d) - x_{d,j}(t_d)\|^2 \ge E^2, \;\; \forall t_d \in [0, t^*_d]. \tag{3}$$

□

b) second, given the geometric curve $x_{d,i}(t_d)$ defined above, and letting the *virtual time* be
$$\gamma_i : \mathbb{R}^+ \to [0, t^*_d] \,, \quad \forall i = 1\,, \dots, n\,, \tag{4}$$
we express the desired position of the i-th UAV at time t as $x_{d,i}(\gamma_i(t))$. In this formulation, the virtual time $\gamma_i(t)$ is a function that maps actual (clock) time t to mission planning time t_d. We notice that, if $\dot\gamma_i(t) = 1$, then the commanded speed coincides with the speed profile chosen at the step **a)** (i.e. $\dot\gamma_i = 1$ implies that the mission is executed at the desired pace). On the other hand, $\dot\gamma_i > 1$ ($\dot\gamma_i < 1$) implies a faster (slower) execution of the mission. As will become clear later on, we explicitely control the dynamics of $\gamma_i(t)$ (actually its second derivative $\ddot\gamma_i(t)$) and use them as an extra degree-of-freedom to achieve time-coordination. Therefore, since $\ddot\gamma_i(t)$ is governed by some control law (yet to be defined), the dynamic constraints on the speed and acceleration of the vehicle, as well as the bounds given in (1a) and (1b) must be considered in order to derive feasibility limits on $\dot\gamma_i(t)$ and $\ddot\gamma_i(t)$. These limits can be determined by deriving the following expression
$$\|\dot x_{d,i}(t)\| = \left\| \frac{dx_{d,i}(\gamma_i)}{d\gamma_i} \frac{d\gamma_i}{dt} \right\| = \left\| x'_{d,i}(t_d)\dot\gamma_i(t) \right\| \,, \tag{5}$$
where $\dot x_{d,i}(t) = d(x_{d,i}(\gamma_i(t)))/dt$ denotes the commanded speed profile to be tracked by the UAV at time t, while $x'_{d,i}(t_d) = dx_{d,i}(\gamma_i)/d\gamma_i$ represents the speed profile generated by the trajectory-generation algorithm [26]. Hence, $\|\dot x_{d,i}(t)\|$ is limited to the physical speed constraints of the vehicle:
$$v_{i,\min} \le \|\dot x_{d,i}(t)\| \le v_{i,\max} \,.$$
Using (5), these speed constraints result in the following inequalities:
$$\dot\gamma_{i,\min}\, v_{d_i,\min} \ge v_{i,\min} \,, \tag{6a}$$
$$\dot\gamma_{i,\max}\, v_{d_i,\max} \le v_{i,\max} \,. \tag{6b}$$
Equations (6a) and (6b) relate the limits of the desired speed profile $x'_{d,i}(t_d)$ to the limits of $\dot\gamma_i(t)$.

Similar limits can be derived for the acceleration profile $\ddot x_{d,i}(t)$. In fact, differentiating Equation (5), and imposing the following upper bound on the required acceleration
$$\|\ddot x_{d,i}(t)\| \le a_{i,\max} \,,$$
we get similar inequalities as (6) for the acceleration and $\ddot\gamma_i(t)$:
$$|\ddot\gamma_{i,\max}\, v_{d_i,\max} + \dot\gamma^2_{i,\max}\, a_{d_i,\max}| \le a_{i,\max} \,. \tag{7}$$
Equation (7) relates the limits of the desired speed and acceleration profiles $x'_{d,i}(t_d)$ and $x''_{d,i}(t_d)$ to the limits of $\dot\gamma_i(t)$ and $\ddot\gamma_i(t)$.

B. 3D Path Following

In what follows, we briefly describe the path-following problem and define a set of variables and assumptions which will be used later in Section IV. Let $\mathcal{I}$ denote an inertial reference frame, and let $x_i(t) \in \mathbb{R}^3$ be the position of the center-of-mass of the i-th multirotor in this inertial frame, resolved in $\mathcal{I}$. Also, let $\mathcal{B}_i = \{\vec b_1, \vec b_2, \vec b_3\}$ denote the body frame with its origin located at the center of mass of the i-th multirotor; vector $\vec b_3$ is the normal to the plane defined by the centers of the rotors –pointing upwards in non-inverted flight–, while vectors $\vec b_1$ and $\vec b_2$ lie in this plane, with $\vec b_1$ pointing out the nose and $\vec b_2$ completing the right-hand system. Recall that $x_{d,i}(\gamma_i(t))$ is the desired position of the i-th vehicle at time t. We define the position error vector as
$$e_{x,i} = x_{d,i} - x_i \;\in \mathbb{R}^3 \tag{8}$$
and the velocity error vector as
$$e_{v,i} = \dot x_{d,i} - \dot x_i \;\in \mathbb{R}^3 \,. \tag{9}$$
Additionally, motivated by [29], we define the error
$$e_{\tilde R,i} = \frac{1}{2}\left(R^\top_{d,i} R_i - R^\top_i R_{d,i}\right)^\vee \,, \tag{10}$$
where $(\cdot)^\vee : \mathfrak{so}(3) \to \mathbb{R}^3$ is the *vee map* defined in [29] mapping the non-zero entries of a skew-symmetric matrix into a three-dimensional vector; $R_i \in \mathsf{SO}(3)$ is the rotation matrix from the body-fixed frame $\mathcal{B}_i$ to the inertial frame $\mathcal{I}$; $R_{d,i} \in \mathsf{SO}(3)$ represents the desired attitude of the i-th multirotor with respect to the inertial frame and is defined as a function of the position and velocity error vectors, $e_{x,i}$ and $e_{v,i}$ [29]. With the above notation, we define the path-following generalized error vector
$$x_{PF,i} = \left[e^\top_{x,i}\,,\; e^\top_{v,i}\,,\; e^\top_{\tilde R,i} \right]^\top \;\in \mathbb{R}^9 \,. \tag{11}$$

The dynamics of the i-th vehicle's path-following error vector can be modeled as

$$\dot{x}_{PF,i} = f_i(x_{PF,i}, u_i, \gamma_i, \dot{\gamma}_i, \ddot{\gamma}_i)\,, \tag{12}$$

where $f_i(\cdot)$ is a general nonlinear vector map and $u_i(t)$ is the path-following control input vector. Finally, $\gamma_i(t)$, $\dot{\gamma}_i(t)$ and $\ddot{\gamma}_i(t)$ can be considered as (known) exogenous signals (as will become clear later, $\gamma_i(t), \dot{\gamma}_i(t)$ and $\ddot{\gamma}_i(t)$ play a crucial role in the time-coordination problem, with $\ddot{\gamma}_i(t)$ being the coordination control input). With this notation, the path-following control problem can be defined as follows:

Problem 2 (Path-Following Problem): Assume that a given i-th multirotor UAV is equipped with a trajectory-generation algorithm that solves Problem 1. Assume that the time derivatives of $x_{d,i}(\gamma_i(t))$ (i.e. the desired reference at time t) are bounded as follows

$$0 \leq v_{i,\text{min}} \leq ||\dot{x}_{d,i}(t)|| \leq v_{i,\text{max}}, \quad ||\ddot{x}_{d,i}(t)|| \leq a_{i,\text{max}}, \tag{13}$$

for all $t \geq 0$. The objective is to determine a control law for $u_i(t)$ such that the generalized path-following error vector $x_{PF,i}(t)$, with the dynamics described in (12), converges to a neighborhood of zero.

In [28] the authors formulate path-following control laws such that the path-following error converges exponentially to zero. Furthermore, it is proven that, in the presence of non-ideal performance of an onboard inner-loop autopilot, the controller exhibits uniformly bounded performance. In other words, the controller $u_i(t)$ in [28] implies that there exists a positive constant c, and for every $a \in (0, c)$, there exists $\rho = \rho(a) > 0$ such that

$$||x_{PF}(0)|| \leq a \implies ||x_{PF}(t)|| \leq \rho \quad \forall t \geq 0\,, \tag{14}$$

with $x_{PF} = [x_{PF,1}^\top, \ldots, x_{PF,n}^\top]^\top \in \mathbb{R}^{9n}$ [30]. □

Remark 1: Notice that, in light of the argument made in Section II-A, the bounds given in (13) are satisfied if inequalities (6) and (7) hold. The latter inequalities depend on the dynamic constraints imposed on the generated trajectory (i.e. $v_{d_i,\text{min}}$, $v_{d_i,\text{max}}$ and $a_{d_i,\text{max}}$ introduced in (1)), as well as on the dynamics of $\gamma_i(t)$ (recall that $\ddot{\gamma}_i(t)$ will be used later at the time-coordination level). For this reason, in the Appendix we show that the control law, which governs $\ddot{\gamma}_i(t)$, and its time integral $\dot{\gamma}_i(t)$, are limited within certain bounds, so that inequalities (6) and (7) are always satisfied. □

III. Time-Coordination: Problem Formulation

We now address the time-coordination problem of a fleet of n multirotor UAVs. As already mentioned earlier, this problem will be solved by adjusting –for each vehicle– the second derivative of the parameterizing variable $\gamma_i(t)$. In what follows, we first define the objective of time-coordination; second, we formulate a set of assumptions on the supporting communication network; finally, we introduce the time-coordination error states and give a formal statement of the problem at hand.

A. Definition of the Time-Coordination Objective

Recall from Section II that the desired position assigned to the i-th vehicle at time t is given by $x_{d,i}(\gamma_i(t))$, where $x_{d,i}(\cdot)$ is the geometric path produced by the trajectory-generation algorithm, and the path parameter $\gamma_i(t)$ is the virtual time defined in (4). As it will become clear later, the virtual time and its first time derivative play a crucial role in the time-coordination problem. In fact, since the desired path assigned to each vehicle is parameterized by $\gamma_i(t)$, we say that if

$$\gamma_i(t) - \gamma_j(t) = 0\,, \quad \forall i, j \in \{1, \ldots, n\}\,, \quad i \neq j\,, \tag{15}$$

then, at time t, all the vehicles are coordinated. Moreover, as already discussed in Section II, if

$$\dot{\gamma}_i(t) - 1 = 0\,, \forall i \in \{1, \ldots, n\}\,, \tag{16}$$

then the desired speed at which the vehicles are required to converge, is equal to the desired speed profile established at the trajectory-generation level. Thus, Equations (15) and (16) capture the objective of vehicle coordination, and a control law for $\ddot{\gamma}_i(t)$ must be formulated to ensure convergence to this equilibrium.

B. Communication Network: Assumptions

To achieve the time-coordination objective, information must be exchanged among the vehicles over a supporting communication network. Using tools from algebraic graph theory, we can model the information flow as well as the constraints imposed by the communication topology. The reader is referred to [31] for key concepts and details on algebraic graph theory.

Let $L(t) \in \mathbb{R}^{n\times n}$ be the Laplacian of the graph $\Gamma(t)$. Let $Q_n \in \mathbb{R}^{(n-1)\times n}$ be a matrix such that $Q_n 1_n = 0$ and $Q_n (Q_n)^\top = I_{n-1}$, with 1_n being a vector in $\mathbb{R}^n$ whose components are all 1.

Remark 2: We notice that a matrix Q_k satisfying $Q_k 1_k = 0$ and $Q_k (Q_k)^\top = I_{k-1}$ can be found recursively as follows:

$$Q_k = \begin{bmatrix} \sqrt{\frac{k-1}{k}} & -\frac{1}{\sqrt{k(k-1)}} 1_{k-1}^\top \\ 0 & Q_{k-1} \end{bmatrix},$$

with initial condition $Q_2 = [\,\frac{1}{\sqrt{2}} \; -\frac{1}{\sqrt{2}}\,]$. For simplicity, from now on we let $Q \triangleq Q_n$, where n is the number of vehicles involved in the cooperative mission. □

Finally, define $\bar{L}(t) \triangleq QL(t)Q^\top \in \mathbb{R}^{(n-1)\times(n-1)}$ (it can be shown that $\bar{L}(t)$ has the same spectrum as the Laplacian $L(t)$ without the eigenvalue $\lambda_1 = 0$ corresponding to the eigenvector 1_n). Given the above notation, we can formulate the following assumptions:

Assumption 1: The i-th UAV communicates only with a neighboring set of vehicles, denoted by $\mathcal{N}_i(t)$.

Assumption 2: The communication between two UAVs is bidirectional with no time delays.

Assumption 3: Matrix $\bar{L}(t)$ satisfies the (normalized) persistency of excitation (PE)-like assumption [32]:

$$\frac{1}{nT} \int_t^{t+T} \bar{L}(\tau) d\tau \geq \mu I_{n-1}\,, \tag{17}$$

where the parameters $T > 0$ and $\mu \in (0,1]$ represent a measure of the level of connectivity of the communication graph. Note that $\mu \in (0,1]$ follows from the fact that $||\bar{L}|| \leq n$ [34].

Remark 3: We note that the PE-like condition (17) requires the communication graph $\Gamma(t)$ to be connected only in an integral sense, not pointwise in time. As a matter of fact, the graph may be disconnected during some interval of time or may even fail to be connected at all times. In this sense, it is general enough to capture packet dropouts, loss of communication, and switching topologies. □

C. Time-Coordination Problem

Let $\gamma(t) = [\gamma_1(t), \ldots, \gamma_n(t)]^\top$, and define the coordination error vectors as

$$\xi(t) = Q\gamma(t) \qquad \in \mathbb{R}^{n-1}, \tag{18}$$

$$z(t) = \dot{\gamma}(t) - 1_n \qquad \in \mathbb{R}^{n}. \tag{19}$$

From the definition of Q it follows that, if $\xi(t) = 0_{n-1}$, then $\gamma_i - \gamma_j = 0$, $\forall i, j \in \{1, \ldots, n\}$. Furthermore, convergence of $z(t)$ to zero implies that the individual coordination variables $\gamma_i(t)$ evolve at the desired rate 1.

With the above notation, the time-coordination problem can now be defined as follows:

Problem 3 (Time-Coordination Problem): Consider a set of n multirotor UAVs equipped with a trajectory-generation algorithm that solves Problem 1, and a path-following control law that solves Problem 2 for any desired reference $x_{d,i}(\gamma_i(t))$ satisfying (13). Then, the objective of time-coordination is to design feedback control laws for $\ddot{\gamma}_i(t)$ for all vehicles such that the time-coordination error vectors $\xi(t)$ and $z(t)$, defined in (18) and (19) respectively, converge to a neighborhood of zero, and such that inequalities (6) and (7) are not violated. □

IV. Main Result

To solve the time-coordination problem, we let the evolution of $\gamma_i(t)$ be given by

$$\ddot{\gamma}_i = -b(\dot{\gamma}_i - 1) - a\sum_{j\in\mathcal{N}_i}(\gamma_i - \gamma_j) - \bar{\alpha}_i(x_{PF,i}),$$

$$\gamma_i(0) = 0, \quad \dot{\gamma}_i(0) = 1,$$

where a and b are positive coordination control gains, while $\bar{\alpha}_i(x_{PF,i})$ is defined as

$$\bar{\alpha}_i(x_{PF,i}) = \frac{\dot{x}_{d,i}(t)^\top e_{x,i}}{\|\dot{x}_{d,i}(t)\| + \delta},$$

with δ being a positive design parameter. The dynamics of $\gamma(t)$ can be written in compact form as

$$\ddot{\gamma} = -bz - aL\gamma - \bar{\alpha}(x_{PF}), \quad \gamma(0) = 0_n, \; \dot{\gamma}(0) = 1_n, \tag{20}$$

where

$$x_{PF} = [x_{PF,1}^\top, \ldots, x_{PF,n}^\top]^\top \qquad \in \mathbb{R}^{9n},$$

$$\bar{\alpha}(x_{PF}) = [\bar{\alpha}_1(x_{PF,1}), \ldots, \bar{\alpha}_n(x_{PF,n})]^\top \qquad \in \mathbb{R}^{n}.$$

Remark 4: The coordination control law given in Equation (20) comprises of three terms. The contribution given by the first term (i.e. $-bz$) allows the UAVs to converge to the desired speed profile (convergence to the equilibrium given in Equation (16)). The second term (i.e. $-aL\gamma$) ensures that the desired position of each UAV satisfies the coordination requirement introduced in Equation (15) (i.e. the UAVs are synchronized at time t). Finally, the third term (i.e. $\bar{\alpha}(x_{PF})$) depends on the path-following error. By virtue of the path-following dependent term , if for example one vehicle is away from the desired position ($||e_x|| \neq 0$), then the other vehicles involved in the cooperative mission adjust their speeds (slow down or speed up) to maintain coordination. This point will become clear in the Simulation Results section.

The following theorem summarizes the main result of this paper.

Theorem 1: Consider a set of n multirotor UAVs equipped with a trajectory-generation algorithm that solves Problem 1. Assume there exists a path-following controller which guarantees that the path-following error satisfies the bound given in (14) for any desired reference $x_{d,i}(\gamma_i(t))$ satisfying (13). Assume that the vehicles communicate over a network satisfying the PE-like assumption (17), and let the time-coordination error vector $x_{TC} = [\xi^\top, z^\top]^\top$ at time $t = 0$ and the path-following performance bound ρ introduced in Problem 2, satisfy

$$\max(||x_{TC}(0)||, \rho) \leq \min\left(\frac{1 - \frac{v_{i,\min}}{v_{d,\min}}}{(\kappa_1 + \kappa_2)}, \right.$$
$$\left. \frac{\frac{v_{i,\max}}{v_{d,\max}} - 1}{(\kappa_1 + \kappa_2)}, \frac{\sqrt{\frac{a_{i,\max}}{a_{d,\max}}} - 1}{(\kappa_1 + \kappa_2)}, \frac{a_{i,\max} - \dot{\gamma}_{i,\max}^2 a_{d,\max}}{v_{d,\max}(b\kappa_1 + b\kappa_2 + 1)}\right). \tag{21}$$

where κ_1 and κ_2 are some positive constants defined in Equations (34) and (35). Finally, let $\ddot{\gamma}(t)$ be governed by (20). Then, there exist control gains a, b, and δ such that the time-coordination is uniformly bounded. In particular, the time-coordination error satisfies

$$||x_{TC}(t)|| \leq \kappa_1 ||x_{TC}(0)|| e^{-\lambda_{TC} t} + \kappa_2 \sup_{t\geq 0}(||x_{PF}(t)||), \tag{22}$$

with

$$\lambda_{TC} < \gamma_\lambda, \quad \gamma_\lambda \geq \bar{\gamma}_\lambda \triangleq \frac{a}{b}\frac{n\mu}{T(1 + \frac{a}{b}nT)^2}. \tag{23}$$

Remark 5: Notice that the maximum convergence rate $\bar{\gamma}_\lambda$ is obtained when the control gains a and b satisfy

$$\frac{a}{b} = \frac{1}{nT}. \tag{24}$$

Substituting (24) in (23), one obtains

$$\max_{a,b>0}(\bar{\gamma}_\lambda) = \frac{\mu}{4T^2},$$

i.e. the rate of convergence depends on the quality of the network only.

Corollary 1: If the path-following error converges exponentially fast to zero with some positive rate of convergence λ_{PF}:

$$||x_{PF}(t)|| \leq k_{PF} ||x_{PF}(0)|| e^{-\lambda_{PF} t},$$

then the time-coordination error converges to zero as follows:

$$||x_{TC}(t)|| \leq \bar{\kappa}_1 ||x_{TC}(0)|| e^{-\lambda_{TC} t} + \bar{\kappa}_2 ||x_{PF}(0)|| e^{-\frac{\lambda_{PF}+\lambda_{TC}}{2} t}, \tag{25}$$

with positive constants $\bar{\kappa}_1$ and $\bar{\kappa}_2$ defined in Equation (41). □

Proof. The proofs of Theorem 1 and Corollary 1 are given in the Appendix. □

Remark 6: We notice that if the desired trajectories $x_{d,i}(\cdot)$ satisfy the temporal separation requirement, i.e. Equation (3), then the result given in Theorem 1 ensures inter-vehicle collision avoidance. In fact, upon knowledge of (i) the quality of service of the communication network (i.e. μ and T in Equation (17)) and (ii) the performance of the given path-following controller (see Equation (14)), one can choose E in Equation (3) large enough so as to guarantee that the vehicles will never collide throughout the mission.

V. Simulation Results

In this section we present simulation results for a scenario in which eight quadrotor UAVs, initially positioned along the perimeter of a $40m \times 40m$ square room, have to exchange their positions while maintaining constant equal height, and arrive at their final destinations at the same time. Before the mission starts, a set of trajectories are generated which ensure temporal deconfliction ($E = 1m$) of the UAVs throughout the mission. Figure 3 depicts the 2D projection of these trajectories (solid lines).

In the remainder of this section, we analyze and validate the theoretical findings through three different simulations. In the first simulation we consider the case of ideal all-to-all communication between the vehicles, and assume that the UAVs' positions coincide with their desired positions for all time, i.e. $||x_{PF}(t)|| = 0\,, \quad \forall t \geq 0$. In the second simulation, we replicate the experiment with non-ideal communication. In the third simulation, we add a bounded path-following error. In all the experiments, the control gains are chosen to be $a = 1.5\,, b = 3.6\,, \delta = 3$. To illustrate the convergence properties of the solution, the virtual times are initialized as follows: $\gamma_1(0) = 2\,, \gamma_4(0) = 3\,, \gamma_6(0) = 1\,, \gamma_8(0) = 1.5\,, \gamma_2(0) = \gamma_3(0) = \gamma_5(0) = \gamma_7(0) = 0$.

A. Ideal Communication - Ideal Path Following

In this simulation, all the vehicles communicate with each other for all time, i.e.

$$l_{ij} = \begin{cases} 7 & \text{for } i = j \\ -1 & \text{for } i \neq j \end{cases},$$

where $l_{ij}(t)'s$ are the entries of the Laplacian matrix $L(t)$. Moroever, we let $||x_{PF}(t)|| = 0\,, \forall t \geq 0$, i.e. the path-following algorithm exhibits ideal performance.

At time $t = 0$ the vehicles start the mission and follow the predefined trajectories until they reach their final destination, at time $t \approx 8.8s$. In Figure 3, the solid lines indicate the trajectories of each UAV, while ICi and FCi indicate, respectively, initial and final position of UAVi.

In Figure 4 the coordination variables are illustrated. At the beginning, vehicles $1, 4, 6$ and 8 speed up, while vehicles $2, 3, 5$ and 7 slow down (see Figure 4b and 4c) until, at time $t \approx 2s$, coordination is achieved. Figure 4a shows convergence of the virtual times to the same increasing value.

B. Non-ideal Communication - Ideal Path-Following

The same experiment is repeated, but in this case, to simulate switching topologies, we let UAVi and UAVj communicate with each other at time $t \geq 0$ only if $||x_i(t) - x_j(t)|| \leq 20m$. Figure 5 depicts an estimate of the quality of service of the network computed as

$$\hat{\mu}(t) = \lambda_{\min}\left(\frac{1}{n}\frac{1}{T}\int_{t-T}^{t} \bar{L}(\tau)d\tau\right)\,, \quad t \geq T\,,$$

with $n = 8$ and $T = 1s$. As can be seen in the figure, the estimate of the quality of service is highest around $t \approx 4 - 5s$, when the vehicles are positioned around the center of the room, thus all close to each other. On the other hand, the value is smaller at the begin and end of the mission, when the vehicles communicate with only a few neighbors. Figure 6 depicts the performance of the time-coordination algorithm. It can be noted that the time-coordination variables converge to the desired values at time $t \approx 4s$, slower than the case with ideal communication.

C. Non-ideal Communication - Non-ideal Path-Following

In this last experiment, to simulate bounded path-following error, we implemented the path-following control law described in [28], and added bounded disturbances at the control input (angular velocities and total thrust). In [28] the authors show that, in the presence of disturbances at the input, the path-following error is ultimately bounded ([28] solves Problem 2). The communication topology is the one used in the previous experiment (Subsection V-B).

The vehicles start, at $t = 0$, with an initial displacement from the desired positions, and track the desired paths. In Figure 3 the dashed lines indicate the actual trajectories of the UAVs. Figure 7 shows the time history of the time-coordination variables. Figure 8 depicts the time history of the norm of the time-coordination error state $||x_{TC}(t)||$ (green line), and compares it with the two cases described above (blue and red lines). As expected, the coordination error converges to a neighborhood of the origin, and remains bounded.

Finally, Figure 9 shows the distance between the vehicles throughout the mission, which is

$$||x_i(t) - x_j(t)||\,, \tag{26}$$

in three different cases: (i) blue line - ideal path-following performance; (ii) green line - the path-following error is introduced, and the time-coordination control law given in (20) is employed; (iii) red line - the path-following error is introduced, and the coordination law employed does not depend on the path-following error (i.e. Equation (20) without the third term $\bar{\alpha}(x_{PF})$). While in case (i) temporal separation is guaranteed at the trajectory generation level, when the UAVs are away from the desired position, the time-coordination algorithm must take into account the path-following error in order to ensure that the actual UAVs' positions are separated.

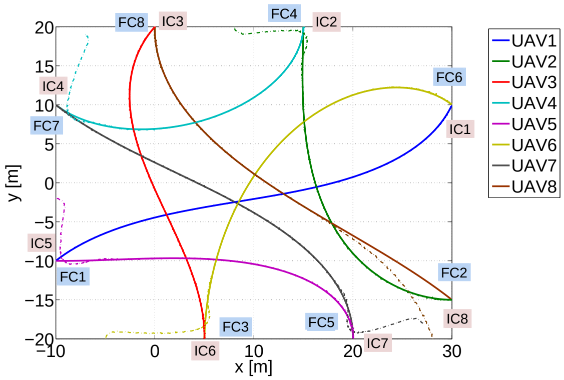

Fig. 3. Simulation results with eight quadrotor UAVs - The solid lines indicate the paths tracked by the UAVs assuming ideal performance of the path-following controller; the dashed lines show the paths tracked by the UAVs when the path-following controller exhibits non ideal performance.

As it was pointed out in Remark 4, the third term in Equation (20) enables the UAVs to maintain coordination even in the presence of path-following errors, which in turns imply that a minimum separation between the vehicles is guaranteed. As it can be seen from Figure 7b and 7c, since UAV8 is initially displaced by a considerable distance from its desired position, when the mission starts the virtual time associated with UAV8 (i.e. γ_8) decelerates significantly ($\dot{\gamma}_8 < 1$ and $\ddot{\gamma}_8 < 0$) by virtue of $\bar{\alpha}(x_{PF})$, to allow the vehicle to approach the desired point faster. As a consequence, also γ_1 decelerates to coordinate with γ_8, thus allowing the actual vehicles to synchronize with each other along the paths and maintain a desired separation. In absence of the term $\bar{\alpha}(x_{PF})$, the virtual times associated with the vehicles would keep coordinating with each other without accounting for the actual position of the UAVs, thus leading to potential collisions (red line in Figure 9).

VI. Flight Test Results

In this section, we present flight test results[2] of two AR.Drone quadrotors that are tasked to follow circular, planar paths of radius 2 m at a constant speed, while synchronizing both their phase-on-orbit and their headings. The trajectory-generation, path-following, and time-coordination control algorithms run in MATLAB\Simulink. Path-following commands are sent to the UAVs at a frequency rate of approximately 30Hz. Position and velocity feedback is provided by a Vicon Motion Capture System at a rate of approximately 100Hz. The coordination variables are exchanged among the UAVs at a data transfer rate of 100Hz (imposed via Simulink).

We refer to the path-following algorithm described in [27] and the time-coordination control law proposed in Section IV. The control gains used in this flight tests are $a = 3$, $b = 5$, $\delta = 5$. Figure 10 presents the results of this experiment. In particular, Figure 10a shows the desired orbit (black) and the actual trajectories of the two quadrotors (blue and red). Since the two UAVs are tasked to follow the same orbit, a phase-on-orbit separation is required between the two vehicles to avoid collision. This separation is specified online from the ground station, and it varies according to mission requirements. The desired phase-on-orbit separation, along with the actual phase separation between the two UAVs, is shown in Figure 10b. In this particular scenario, the UAVs are initially required to keep a 180-deg phase separation; at approximately $t = 94$ s, the required phase separation goes down to 90 deg; the two quadrotors keep this configuration for about 14 s, when the required phase separation goes back to 180 deg; finally, in the last part of the experiment, the UAVs are required to keep a phase separation of 270 deg. Figure 10c shows the convergence of $\dot{\gamma}_1$ and $\dot{\gamma}_2$ to the desired rate 1, as well as the convergence of the coordination errors to a neighborhood of

[2]For a thorough description of the setup used in these flight tests, as well as guidelines and implementation details, the reader is referred to http://naira.mechse.illinois.edu/quadrotor-uavs/

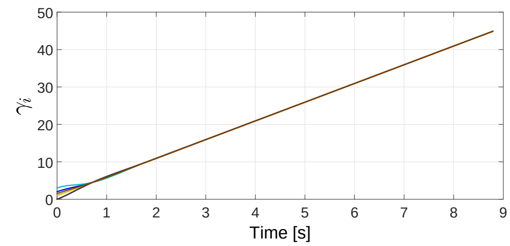

(a) Virtual time.

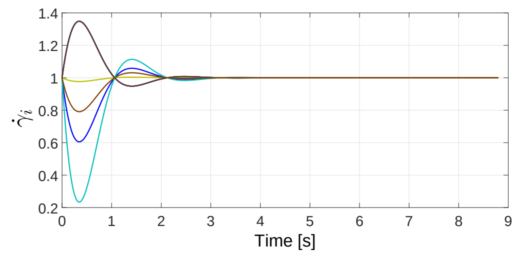

(b) Derivative of virtual time.

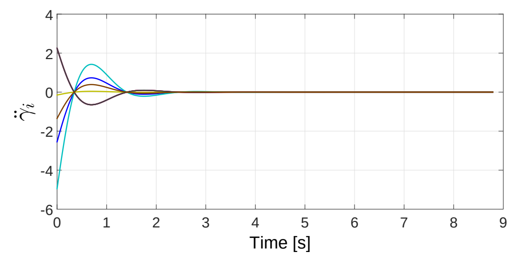

(c) Control input.

Fig. 4. Time-coordination in the case of ideal communication and ideal path-following performance. (a) Convergence of γ_i's to the same increasing value. (b) Convergence of $\dot{\gamma}_i$'s to 1. (c) Time Coordination Control Input.

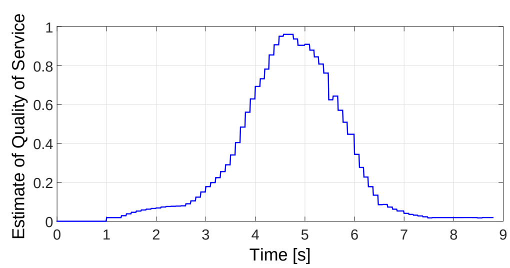

Fig. 5. Estimate of the quality of service computed as $\hat{\mu}(t) = \lambda_{\min}\left(\frac{1}{n}\frac{1}{T}\int_{t-T}^{t}\bar{L}(\tau)d\tau\right)$, $t \geq T$.

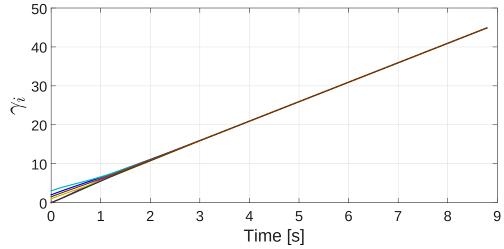

(a) Virtual time.

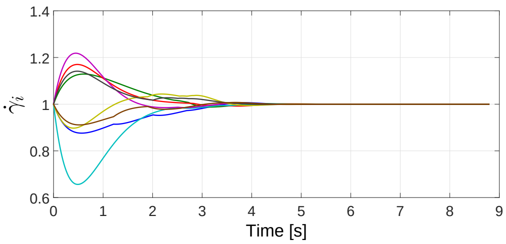

(b) Derivative of virtual time.

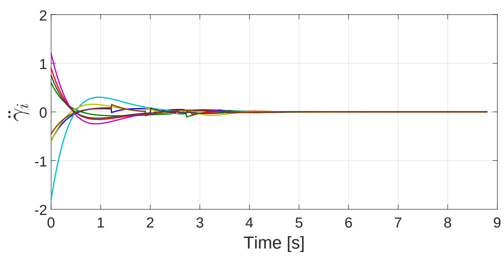

(c) Control input.

Fig. 6. Time-coordination in the case of non-ideal communication and ideal path-following performance. (a) Convergence of γ_i's to the same increasing value. (b) Convergence of $\dot{\gamma}_i$'s to 1. (c) Time Coordination Control Input.

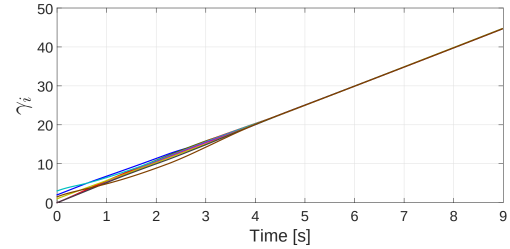

(a) Virtual time.

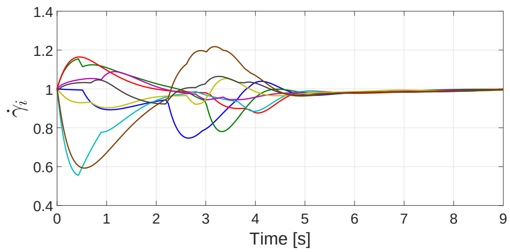

(b) Derivative of virtual time.

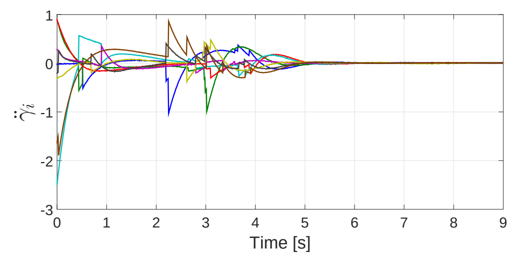

(c) Control input.

Fig. 7. Time-coordination in the case of non-ideal communication and non-ideal path-following performance. (a) Convergence of γ_i's to the same increasing value. (b) Convergence of $\dot{\gamma}_i$'s to 1. (c) Time Coordination Control Input.

zero. [3]

VII. Conclusions

This paper addressed the problem of time coordination for a fleet of multirotor UAVs along predefined spatial paths according to mission requirements. With the solution proposed, cooperative control is achieved in the presence of time-varying communication networks, as well as stringent temporal constraints, such as simultaneous arrival at the desired final locations. The proposed solution solves the time-coordination problem under the assumption that the trajectory-generation and the path-following algorithms —meeting certain stability conditions— are given. The coordination task is accomplished by adjusting an appropriately defined coordination variable. The convergence of the time-coordination error vector to a neighborhood of zero is demonstrated using Lyapunov analysis. Simulations and flight test results were presented to validate the developed algorithms. Future works by the research group will address directed communication graphs, time-delayed communication, as well as the development of collision-avoidance algorithms to ensure safety even in the presence of static and dynamic pop-up obstacles..

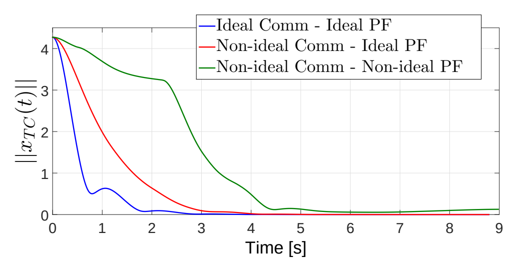

Fig. 8. Time-coordination error vector.

Appendix A
Proof of Theorem 1

Consider the following system

$$\dot{\phi}(t) = -\frac{a}{b}\bar{L}\phi(t)\,, \tag{27}$$

where the matrix $\bar{L}$ satisfies the (PE)-like condition in (17). Then, using the result reported in [35, Lemma 5], we conclude that the system in (27) is GUES (globally uniformly exponentially stable), and that the following bound holds:

$$||\phi(t)|| \leq k_\lambda ||\phi(0)||e^{-\gamma_\lambda t}$$

[3]Video available at http://naira.mechse.illinois.edu/quadrotor-uavs/. At http://www.youtube.com/watch?v=OBtLCf1Lfiw, a video of two quadrotors coordinating along with a tango song is presented. In this example, the sound wave of the song plays the role of a *virtual vehicle* with which the quadrotors are required to coordinate (absolute temporal constraints). Further details regarding this experiment can be found in the description of the video.

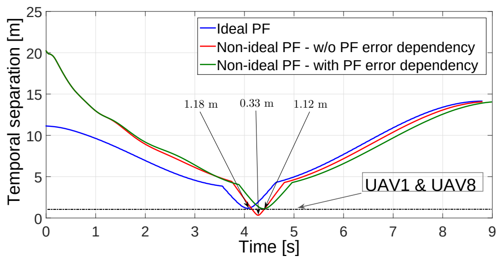

Fig. 9. Temporal separation between the vehicles.

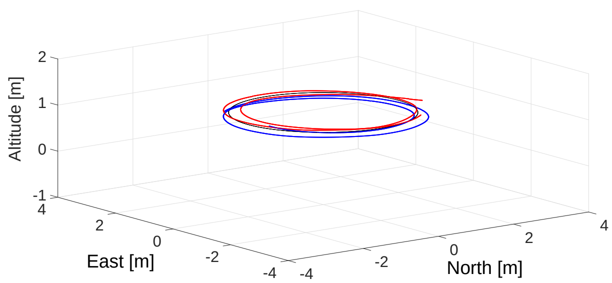

(a) Desired (black circle) and actual (red and blue lines) orbits.

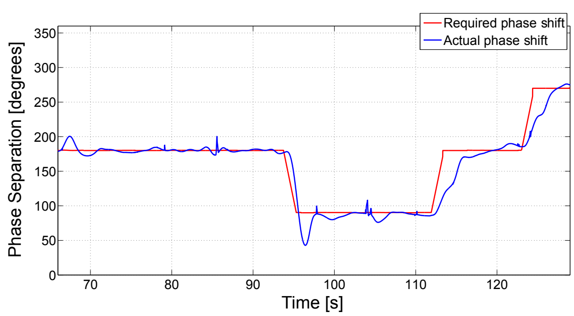

(b) Desired (red line) and actual (blue line) phase separation.

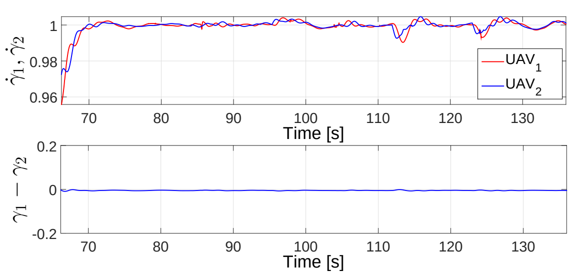

(c) Coordination errors computed as $\dot\gamma_1 - \dot\gamma_2$ and $\gamma_1 - \gamma_2$.

Fig. 10. Flight test results with two AR.Drone UAVs.

with $k_\lambda = 1$ and $\gamma_\lambda \geq \bar\gamma_\lambda = \frac{a}{b}\frac{n\mu}{T(1+\frac{a}{b}nT)^2}$. This, together with [35, Lemma 1] or a similar argument as the one in [30, Theorem 4.14], implies that there exists a continuously differentiable, symmetric, positive definite matrix $P(t)$ that satisfies the inequalities

$$0 < \bar c_1 I \triangleq \frac{\bar c_3}{2n} I \leq P(t) \leq \frac{\bar c_4}{2\gamma_\lambda} I \triangleq \bar c_2 I$$
$$\dot P - \frac{a}{b}\bar L P - \frac{a}{b} P \bar L \leq -\bar c_3 I\,. \tag{28}$$

Next, introducing the vector

$$\chi(t) = b\xi(t) + Qz(t)\,,$$

the time-coordination states can be redefined as $\bar x_{TC} = [\chi^\top, z^\top]^\top$, with dynamics

$$\begin{cases}\dot\chi = -\frac{a}{b}\bar L\chi + \frac{a}{b}QLz - Q\bar\alpha(x_{PF}) \\ \dot z = -(bI - \frac{a}{b}L)z - \frac{a}{b}LQ^\top\chi - \bar\alpha(x_{PF})\,.\end{cases} \tag{29}$$

Consider the following Lyapunov candidate function

$$V = \chi^\top P\chi + \frac{\beta_1}{2}||z||^2 = \bar x_{TC}^\top W \bar x_{TC}\,, \tag{30}$$

where $\beta_1 > 0$, P was introduced above, and

$$W = \begin{bmatrix} P & 0 \\ 0 & \frac{\beta_1}{2}\end{bmatrix}.$$

Using (29), the time derivative of (30) can be computed to yield

$$\begin{aligned}\dot V &= \chi^\top P\left(-\frac{a}{b}\bar L\chi + \frac{a}{b}QLz - Q\bar\alpha_{PF}\right) + \\ &+ \left(-\frac{a}{b}\chi^\top\bar L + \frac{a}{b}z^\top LQ^\top - \bar\alpha_{PF}^\top Q^\top\right)P\chi + \\ &+ \chi^\top\dot P\chi + \beta_1 z^\top\left(-\left(bI - \frac{a}{b}L\right)z - \frac{a}{b}LQ^\top\chi - \bar\alpha_{PF}\right),\end{aligned}$$

which leads to

$$\begin{aligned}\dot V \leq{}& \chi^\top\left(\dot P - \frac{a}{b}P\bar L - \frac{a}{b}\bar L P\right)\chi - \beta_1 z^\top\left(bI - \frac{a}{b}L\right)z \\ &+ 2\frac{a}{b}n||P||||\chi||||z|| + 2||P||||\chi||||\bar\alpha_{PF}|| \\ &+ \beta_1\frac{a}{b}n||z||||\chi|| + \beta_1||z||||\bar\alpha_{PF}||\,,\end{aligned}$$

where we used the fact that $||\bar L|| \leq n$ [34, Corollary 13.1.4]. Using (28), and after straightforward computations, we obtain:

$$\begin{aligned}\dot V \leq{}& -\bar c_3||\chi||^2 - \beta_1\left(b - \frac{a}{b}n\right)||z||^2 + \left(2\frac{a}{b}n\bar c_2 + \beta_1\frac{a}{b}n\right)||z||||\chi|| + \\ &+ 2\left(2\bar c_2||\chi|| + \beta_1||z||\right)\frac{v_{\max}}{v_{\min}+\delta}||x_{PF}||\,,\end{aligned}$$

where $v_{\max} = \max_i\{v_{i,\max}\}$, $v_{\min} = \min_i\{v_{i,\min}\}$.

Finally, using $\bar c_2 = \frac{\bar c_4}{2\gamma_\lambda}$, letting $\bar c_4 = \bar c_3$, and choosing $\delta > v_{\max} - v_{\min}$, we get

$$\begin{aligned}\dot V \leq{}& -\bar c_3||\chi||^2 - \beta_1\left(b - \frac{a}{b}n\right)||z||^2 + \left(\frac{a}{b}\frac{n\bar c_3}{\bar\gamma_\lambda} + \beta_1\frac{a}{b}n\right)||z||||\chi|| + \\ &+ 2\left(\frac{\bar c_3}{\bar\gamma_\lambda} + \beta_1\right)\frac{v_{\max}}{v_{\min}+\delta}||x_{PF}||\,,\end{aligned}$$

that can be written in matrix form as

$$\dot V \leq -\bar x_{TC}^\top M\bar x_{TC} + 2\left(\frac{\bar c_3}{\bar\gamma_\lambda} + \beta_1\right)||\bar x_{TC}||||x_{PF}||\,,$$

with

$$M = \begin{bmatrix}\bar c_3 & -\left(\frac{a}{b}\frac{n\bar c_3}{\bar\gamma_\lambda} + \beta_1\frac{a}{b}n\right) \\ -\left(\frac{a}{b}\frac{n\bar c_3}{\bar\gamma_\lambda} + \beta_1\frac{a}{b}n\right) & \beta_1\left(b - \frac{a}{b}n\right)\end{bmatrix}.$$

Next, we note that letting λ_{TC} be some variable that satisfies $\lambda_{TC} < \gamma_\lambda$, we can choose b large enough so that the following matrix inequality holds:

$$\begin{aligned}&M - 2\lambda_{TC}W \geq \\ &\begin{bmatrix}\bar c_3 - \frac{\bar c_3\lambda_{TC}}{\bar\gamma_\lambda} & -\left(\frac{a}{b}\frac{n\bar c_3}{\bar\gamma_\lambda} + \beta_1\frac{a}{b}n\right) \\ -\left(\frac{a}{b}\frac{n\bar c_3}{\bar\gamma_\lambda} + \beta_1\frac{a}{b}n\right) & \beta_1\left(b - \frac{a}{b}n\right) - \beta_1\lambda_{TC}\end{bmatrix} \geq 0\,.\end{aligned} \tag{31}$$

Thus, the derivative of the Lyapunov function is bounded as follows

$$\dot V \leq -2\lambda_{TC}V + 2\left(\frac{\bar c_3}{\bar\gamma_\lambda} + \beta_1\right)||\bar x_{TC}||||x_{PF}||\,.$$

Using [30, Lemma 4.6], one can conclude that the system (29) is input to state stable, with input x_{PF}, and the following bound holds:

$$||\bar{x}_{TC}(t)|| \leq \sqrt{\frac{\max(\bar{c}_2, \beta_1/2)}{\min(\bar{c}_1, \beta_1/2)}} ||\bar{x}_{TC}(0)|| e^{-\lambda_{TC} t} + \sqrt{\frac{\max(\bar{c}_2, \beta_1/2)}{\min(\bar{c}_1, \beta_1/2)}} \frac{\frac{\bar{c}_3}{\bar{\gamma}_\lambda} + \beta_1}{\bar{\gamma}_\lambda \min(\bar{c}_1, \beta_1/2)} \sup_{t \geq 0} (||x_{PF}(t)||) . \quad (32)$$

Finally, from the definition

$$\bar{x}_{TC} \triangleq S x_{TC}, \quad S = \begin{bmatrix} bI_{n-1} & Q \\ 0 & I_n \end{bmatrix},$$

we can conclude that

$$||x_{TC}(t)|| \leq \kappa_1 ||x_{TC}(0)|| e^{-\lambda_{TC} t} + \kappa_2 \sup_{t \geq 0} (||x_{PF}(t)||), \quad (33)$$

with

$$\kappa_1 = ||S^{-1}|| \sqrt{\frac{\max(\bar{c}_2, \beta_1/2)}{\min(\bar{c}_1, \beta_1/2)}} ||S||, \quad (34)$$

and

$$\kappa_2 = ||S^{-1}|| \sqrt{\frac{\max(\bar{c}_2, \beta_1/2)}{\min(\bar{c}_1, \beta_1/2)}} \frac{\frac{\bar{c}_3}{\bar{\gamma}_\lambda} + \beta_1}{\bar{\gamma}_\lambda \min(\bar{c}_1, \beta_1/2)} . \quad (35)$$

As a last step to complete the proof, we need to demonstrate that $\dot{\gamma}_i$ and $\ddot{\gamma}_i$ $\forall i \in \{1 \ldots, n\}$ satisfy the bounds given in (6) and (7). To this end, notice that

$$\ddot{\gamma}_i \leq b||z|| + an||\xi|| + ||x_{PF}|| .$$

For simplicity, let $b > an$. Using the bound in (33), and recalling the bound on the path-following error in (14), the above inequality reduces to

$$\ddot{\gamma}_i \leq (b\kappa_1 + b\kappa_2 + 1) \max(||x_{TC}(0)||, \rho) .$$

Moreover, using the fact that

$$||z(t)|| \leq \kappa_1 ||x_{TC}(0)|| e^{-\lambda_{TC} t} + \kappa_2 \sup_{t \geq 0} (||x_{PF}(t)||),$$

one can show

$$\dot{\gamma}_i \leq 1 + (\kappa_1 + \kappa_2) \max(||x_{TC}(0)||, \rho) ,$$
$$\dot{\gamma}_i \geq 1 - (\kappa_1 + \kappa_2) \max(||x_{TC}(0)||, \rho) .$$

Finally, since by assumption inequality (21) holds, then (6) and (7) are satisfied, and one can show that the bound in (33) holds $\forall t \geq 0$.

APPENDIX B
PROOF OF COROLLARY 1

Assume that the given path-following algorithm satisfies

$$||x_{PF}(t)|| \leq k_{PF} ||x_{PF}(0)|| e^{-\lambda_{PF} t} . \quad (36)$$

Now, rewrite inequality (33) as follows:

$$||x_{TC}(t)|| \leq \kappa_1 ||x_{TC}(s)|| e^{-\lambda_{TC}(t-s)} + \kappa_2 \sup_{s \leq \tau \leq t} (||x_{PF}(\tau)||), \quad (37)$$

where $t \geq s \geq 0$. Apply (37) with $s = t/2$ to obtain

$$||x_{TC}(t)|| \leq \kappa_1 ||x_{TC}(t/2)|| e^{-\lambda_{TC}(t/2)} + \kappa_2 \sup_{t/2 \leq \tau \leq t} (||x_{PF}(\tau)||) . \quad (38)$$

Apply (37) with $s = 0$ and t replaced by $t/2$ to obtain the estimate of $x_{TC}(t/2)$ as

$$||x_{TC}(t/2)|| \leq \kappa_1 ||x_{TC}(0)|| e^{-\lambda_{TC}(t/2)} + \kappa_2 \sup_{0 \leq \tau \leq t/2} (||x_{PF}(\tau)||) . \quad (39)$$

Combining (38) and (39) we get

$$||x_{TC}(t)|| \leq \kappa_1 e^{-\lambda_{TC} t/2} \Big(\kappa_1 ||x_{TC}(0)|| e^{-\lambda_{TC} t/2} + \kappa_2 \sup_{0 \leq \tau \leq t/2} (||x_{PF}(\tau)||) \Big) + \kappa_2 \sup_{t/2 \leq \tau \leq t} (||x_{PF}(\tau)||) . \quad (40)$$

Notice that using (36) we can write

$$\sup_{0 \leq \tau \leq t/2} (||x_{PF}(\tau)||) \leq k_{PF} ||x_{PF}(0)|| ,$$
$$\sup_{t/2 \leq \tau \leq t} (||x_{PF}(\tau)||) \leq k_{PF} ||x_{PF}(0)|| e^{-\lambda_{PF} t/2}$$

Therefore, combining (40) with the previous two inequalities, and letting

$$\bar{\kappa}_1 \triangleq \kappa_1^2, \quad \bar{\kappa}_2 \triangleq (1 + \kappa_1) \kappa_2 k_{PF} , \quad (41)$$

we get

$$||x_{TC}(t)|| \leq \bar{\kappa}_1 ||x_{TC}(0)|| e^{-\lambda_{TC} t} + \bar{\kappa}_2 ||x_{PF}(0)|| e^{-\frac{\lambda_{PF} + \lambda_{TC}}{2} t} ,$$

thus proving Corollary 1.

REFERENCES

[1] M. Mesbahi and F. Y. Hadaegh, “Formation flying control of multiple spacecraft via graphs, matrix inequalities, and switching,” *Journal of Guidance, Control and Dynamics*, vol. 24, no. 2, pp. 369–377, March–April 2001.

[2] M. Saska, V. Vonásek, T. Krajník, and L. Přeučil, “Coordination and navigation of heterogeneous mav–ugv formations localized by a hawk-eye-like approach under a model predictive control scheme,” *The International Journal of Robotics Research*, p. 0278364914530482, 2014.

[3] M. Saska, T. Krajník, V. Vonásek, Z. Kasl, V. Spurnỳ, and L. Přeučil, “Fault-tolerant formation driving mechanism designed for heterogeneous mavs-ugvs groups,” *Journal of Intelligent & Robotic Systems*, vol. 73, no. 1-4, pp. 603–622, 2014.

[4] Y. D. Song, Y. Li, and X. H. Liao, “Orthogonal transformation based robust adaptive close formation control of multi-UAVs,” in *American Control Conference*, vol. 5, Portland, OR, June 2005, pp. 2983–2988.

[5] D. M. Stipanović, G. İnalhan, R. Teo, and C. J. Tomlin, “Decentralized overlapping control of a formation of unmanned aerial vehicles,” *Automatica*, vol. 40, no. 8, pp. 1285–1296, August 2004.

[6] R. Ghabcheloo, A. M. Pascoal, C. Silvestre, and I. Kaminer, “Coordinated path following control of multiple wheeled robots using linearization techniques,” *International Journal of Systems Science*, vol. 37, no. 6, pp. 399–414, May 2006.

[7] B. P. Gerkey and M. J. Matarić, “A formal analysis and taxonomy of task allocation in multi-robot systems,” *The International Journal of Robotics Research*, vol. 23, no. 9, pp. 939–954, 2004.

[8] M. Turpin, N. Michael, and V. Kumar, “Concurrent assignment and planning of trajectories for large teams of interchangeable robots,” in *Robotics and Automation (ICRA), 2013 IEEE International Conference on*, 2013, pp. 842–848.

[9] R. Ghabcheloo, A. P. Aguiar, A. M. Pascoal, C. Silvestre, I. Kaminer, and J. P. Hespanha, “Coordinated path-following control of multiple underactuated autonomous vehicles in presence of communication failures,” in *IEEE Conference on Decision and Control*, San Diego, CA, December 2006, pp. 4345–4350.

[10] F. L. Pereira and J. B. de Sousa, “Coordinated control of networked vehicles: An autonomous underwater system,” *Automation and Remote Control*, vol. 65, no. 7, pp. 1037–1045, July 2004.

[11] U. Gurcuoglu, G. A. Puerto-Souza, F. Morbidi, and G. L. Mariottini, “Hierarchical control of a team of quadrotors for cooperative active target tracking,” in *Intelligent Robots and Systems (IROS), 2013 IEEE/RSJ International Conference on*, 2013, pp. 5730–5735.

[12] R. Ritz and R. D’Andrea, “Carrying a flexible payload with multiple flying vehicles,” in *Intelligent Robots and Systems (IROS), 2013 IEEE/RSJ International Conference on*. IEEE, 2013, pp. 3465–3471.

[13] S. Gupte, P. I. T. Mohandas, and J. M. Conrad, “A survey of quadrotor unmanned aerial vehicles,” in *Southeastcon, 2012 Proceedings of IEEE*. IEEE, 2012, pp. 1–6.

[14] A. Kushleyev, D. Mellinger, C. Powers, and V. Kumar, “Towards a swarm of agile micro quadrotors,” *Autonomous Robots*, vol. 35, no. 4, pp. 287–300, 2013.

[15] J. J. Acevedo, B. C. Arrue, J. M. Diaz-Bañez, I. Ventura, I. Maza, and A. Ollero, "One-to-one coordination algorithm for decentralized area partition in surveillance missions with a team of aerial robots," *Journal of Intelligent & Robotic Systems*, vol. 74, no. 1-2, pp. 269–285, 2014.

[16] J. Capitan, M. T. Spaan, L. Merino, and A. Ollero, "Decentralized multi-robot cooperation with auctioned POMDPs," *The International Journal of Robotics Research*, vol. 32, no. 6, pp. 650–671, 2013.

[17] V. Gazi and K. M. Passino, "A class of attractions/repulsion functions for stable swarm aggregations," *International Journal of Control*, vol. 77, no. 18, pp. 1567–1579, 2004.

[18] V. Gazi, "Swarm aggregations using artificial potentials and sliding-mode control," *IEEE Transactions on Robotics*, vol. 21, no. 6, pp. 1208–1214, 2005.

[19] M. Egerstedt and X. Hu, "Formation constrained multi-agent control," in *IEEE Transaction on Robotics and Automation*. IEEE, 2001, pp. 947–251.

[20] H. Tanner, A. Jadbabaie, and G. Pappas, "Flocking in fixed and switching networks," *IEEE Transactions on Automatic Control*, vol. 52, no. 5, pp. 863–868, 2007.

[21] I. Kaminer, A. M. Pascoal, E. Hallberg, and C. Silvestre, "Trajectory tracking for autonomous vehicles: An integrated approach to guidance and control," *Journal of Guidance, Control and Dynamics*, vol. 21, no. 1, pp. 29–38, January–February 1998.

[22] Y. Kim and M. Mesbahi, "On maximizing the second smallest eigenvalue of state-dependent graph Laplacian," *IEEE Transactions on Automatic Control*, vol. 51, no. 1, pp. 116–120, January 2006.

[23] E. Xargay, I. Kaminer, A. M. Pascoal, N. Hovakimyan, V. Dobrokhodov, V. Cichella, A. P. Aguiar, and R. Ghabcheloo, "Time-critical cooperative path following of multiple UAVs over time-varying networks," *Journal of Guidance, Control and Dynamics*, vol. 36, no. 2, pp. 499–516, March–April 2013.

[24] A. P. Aguiar, J. P. Hespanha, and P. V. Kokotović, "Performance limitations in reference tracking and path following for nonlinear systems," *Automatica*, vol. 44, no. 3, pp. 598–610, March 2008.

[25] R. Ghabcheloo, A. P. Aguiar, A. M. Pascoal, C. Silvestre, I. Kaminer, and J. P. Hespanha, "Coordinated path-following in the presence of communication losses and delays," *SIAM Journal on Control and Optimization*, vol. 48, no. 1, pp. 234–265, 2009.

[26] R. Choe, V. Cichella, E. Xargay, N. Hovakimyan, A. Trujillo, and I. Kaminer, "A trajectory-generation framework for time-critical cooperative missions," in *AIAA Infotech@Aerospace Conference*, Boston, MA, August 2013.

[27] V. Cichella, I. Kaminer, E. Xargay, V. Dobrokhodov, N. Hovakimyan, A. P. Aguiar, and A. M. Pascoal, "A Lyapunov-based approach for time-coordinated 3D path-following of multiple quadrotors," in *IEEE Conference on Decision and Control*, Maui, HI, December 2012, pp. 1776–1781.

[28] V. Cichella, R. Choe, S. B. Mehdi, E. Xargay, N. Hovakimyan, I. Kaminer, and V. Dobrokhodov, "A 3D path-following approach for a multirotor UAV on $\mathsf{SO}(3)$," in *IFAC Workshop RED-UAS*, Compiegne, France, November 2013.

[29] T. Lee, M. Leok, and N. H. McClamroch, "Geometric tracking control of a quadrotor UAV on $\mathsf{SE}(3)$," in *Conference on Decision and Control*, Atlanta, GA, December 2010, pp. 5420–5425.

[30] H. K. Khalil, *Nonlinear Systems*. Englewood Cliffs, NJ: Prentice Hall, 2002.

[31] N. Biggs, *Algebraic Graph Theory*. New York, NY: Cambridge University Press, 1993.

[32] M. Arcak, "Passivity as a design tool for group coordination," *IEEE Transactions on Automatic Control*, vol. 52, no. 8, pp. 1380–1390, August 2007.

[33] Z. Lin, B. A. Francis, and M. Maggiore, "State agreement for continuous-time coupled nonlinear systems," *SIAM Journal on Control and Optimization*, vol. 46, no. 1, pp. 288–307, 2007.

[34] C. Godsil and G. Royle, *Algebraic graph theory*. Springer New York, 2001, vol. 207.

[35] A. Loría and E. Panteley, "Uniform exponential stability of linear time-varying systems: Revisited," *Systems & Control Letters*, vol. 47, no. 1, pp. 13–24, September 2002.

Venanzio Cichella received his M.S. in Automation Engineering in 2011 from the University of Bologna. Before that he spent 9 month at TU Delft as an Erasmus student, and 1 year at the Naval Postgraduate School as a visiting scholar and research assistant. In 2011 he started working on control of autonomous vehicles at the Naval Postgraduate School. In 2012 he moved to the University of Illinois at Urbana-Champaign, where he is currently a Ph.D. candidate in the Department of Mechanical Engineering. In 2015, he received the Ross J. Martin Memorial Award from the College of Engineering at UIUC for outstanding research achievement. His research interests include cooperative control of autonomous aerial and ground robots, nonlinear systems, robust and adaptive control.

Isaac Kaminer received his Ph.D. in Electrical Engineering from University of Michigan in 1992. Before that he spent four years working at Boeing Commercial first as a control engineer in 757/767/747-400 Flight Management Computer Group and then as an engineer in Flight Control Research Group. Since 1992 he has been with the Naval Postgraduate School first at the Aeronautics and Astronautics Department and currently at the Department of Mechanical and Aerospace Engineering where he is a Professor. He has a total of over 20 years of experience in development and flight testing of guidance, navigation and control algorithms for both manned and unmanned aircraft. His more recent efforts were focused on development of coordinated control strategies for multiple UAVs and vision based guidance laws for a single UAV. Professor Kaminer has co-authored more than a hundred refereed publications. Over the years his research has been supported by ONR, NASA, US Army, NAVAIR and USSOCOM.

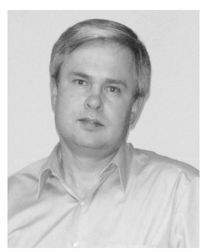

Vladimir Dobrokhodov received his M.S. degrees in astronautical engineering in 1991 and in operations research in 1993 from the Moscow State Aviation Institute and the Air Force Engineering Academy (AFEA), respectively. He earned his Ph.D. in aeronautical and astronautical engineering in 1999, from the Air Force Engineering Academy. Upon finishing his Ph.D. he joined the Flight Dynamics chair at the AFEA as a research scientist. He joined the Naval Postgraduate School (NPS) in February 2001, first as a winner of the United States National Research Council Postdoctoral Fellowship award and then (since 2004) as an Associate Professor of the Mechanical and Aerospace engineering department at the NPS. He has authored/coauthored more than 60 refereed publications. His research interests include flight mechanics and trajectory optimization; guidance, navigation and control with an emphasis on unmanned systems; cooperative control and combat maneuvering of multi-vehicle formations; real-time embedded control systems design.

Enric Xargay received an M.S. in Control Engineering from the Technical University of Catalonia and an M.S. in Aerospace Engineering from the Politecnico di Torino, both in 2007. He earned his Ph.D. in Aerospace Engineering from the University of Illinois at Urbana-Champaign (UIUC) in 2013. Since 2013 he has been with the Department of Mechanical Science and Engineering of UIUC, where he is currently a postdoctoral research associate. In 2011, he received the Roger A. Strehlow Memorial Award from the Department of Aerospace Engineering at UIUC for outstanding research accomplishment. His research interests include aircraft flight control, nonlinear systems, adaptive control, robust control, and cooperative motion planning and control of autonomous systems.

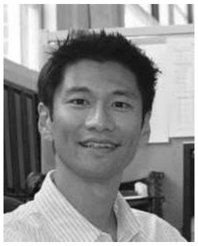

Ronald Choe received his M.Sc. degree in Aerospace Engineering from the Delft University of Technology, The Netherlands in 2002. From 2005-2009 he worked at ST Aerospace and DSO National Laboratories, both in Singapore. Currently he is a Ph.D. candidate in the Department of Aerospace Engineering at the University of Illinois at Urbana-Champaign. His research interests are in the theory of nonlinear and robust adaptive control with applications in (autonomous) aerospace systems, and cooperative trajectory generation and control of multi-vehicle systems.

Naira Hovakimyan received her M.S. degree in Theoretical Mechanics and Applied Mathematics in 1988 from Yerevan State University in Armenia. She got her Ph.D. in Physics and Mathematics in 1992, in Moscow, from the Institute of Applied Mathematics of Russian Academy of Sciences, majoring in optimal control and differential games. In 1997 she has been awarded a governmental postdoctoral scholarship to work in INRIA, France. In 1998 she was invited to the School of Aerospace Engineering of Georgia Tech, where she worked as a research faculty member until 2003. In 2003 she joined the Department of Aerospace and Ocean Engineering of Virginia Tech, and in 2008 she moved to University of Illinois at Urbana-Champaign, where she is a professor, university scholar and Schaller faculty scholar of Mechanical Science and Engineering. She has co-authored a book and more than 300 refereed publications. She is the recipient of the SICE International scholarship for the best paper of a young investigator in the VII ISDG Symposium (Japan, 1996), and also the 2011 recipient of AIAA Mechanics and Control of Flight award. In 2014 she was awarded the Humboldt prize for her lifetime achievements and was recognized as Hans Fischer senior fellow of Technical University of Munich. She is an associate fellow and life member of AIAA, a Senior Member of IEEE, and a member of SIAM, AMS and ISDG. Her research interests are in the theory of robust adaptive control and estimation, control in the presence of limited information, networks of autonomous systems, game theory and applications of those in safety-critical systems of aerospace, mechanical, electrical, petroleum and biomedical engineering.

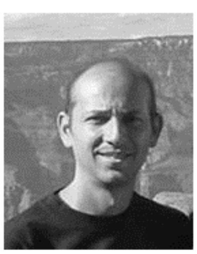

A. Pedro Aguiar received the Licenciatura, M.S. and Ph.D. in electrical and computer engineering from the Instituto Superior Tcnico (IST), Technical University of Lisbon, Portugal in 1994, 1998 and 2002, respectively. Currently, Dr. Aguiar holds an Associate Professor position with the Department of Electrical and Computer Engineering (DEEC), Faculty of Engineering, University of Porto (FEUP). From 2002 to 2005, he was a post-doctoral researcher at the Center for Control, Dynamical-Systems, and Computation at the University of California, Santa Barbara (UCSB). From 2005 to 2012, he was a senior researcher with the Institute for Systems and Robotics at IST (ISR/IST), and an invited assistant professor with the Department of Electrical and Computer Engineering, IST. His research interests include modeling, control, navigation, and guidance of autonomous robotic vehicles, nonlinear control, switched and hybrid systems, tracking, path-following, performance limitations, nonlinear observers, the integration of machine vision with feedback control, networked control, and coordinated/cooperative control of multiple autonomous robotic vehicles.

António M. Pascoal received the Licenciatura degree in electrical engineering from the Instituto Superior Técnico (IST), Lisbon, Portugal in 1974, the M.S. degree in electrical engineering from the University of Minnesota in 1983, and the Ph.D. degree in control science from the same school in 1987. From 1987-88 he was a Research Scientist with Integrated Systems Incorporated, Santa Clara, California, where he conducted research and development work in the areas of system modeling and identification and robust and adaptive control. Since 1998 he has been with the Department of Electrical Engineering of IST, where he is currently an Associate Professor of Control and Robotics and Member, Scientific Council of the Institute for Systems and Robotics, Lisbon. He is also an Adjunct Scientist with the National Institute of Oceanography (NIO), Goa India. He was the Elected Chair, IFAC Technical Committee Marine Systems, from 2008-2014. He has coordinated and participated in a large number of international projects with institutions in Europe, US, India, and Korea, that have led to the design, development, and field-testing of single and multiple autonomous marine and air vehicles. His research interests include linear and nonlinear control theory, robust adaptive control, and networked cooperative motion planning, navigation, and control of multiple autonomous vehicles with applications to air, land, and underwater robots. His long-term goal is to contribute to the development of advanced robotic systems for ocean exploration and exploitation.